JOURNAL OF GEOPHYSICAL RESEARCH, VOL. 102, NO. C2, PAGES 3357–3370, FEBRUARY 15, 1997

A laboratory study of the effect of frost flowers on C band radar backscatter from sea ice

S. V. Nghiem,[1] S. Martin,[2] D. K. Perovich,[3] R. Kwok,[1]
R. Drucker,[2] and A. J. Gow[3]

Abstract. C band images of Arctic sea ice taken by the ERS 1 synthetic aperture radar show transitory regions of enhanced radar backscatter from young sea ice. Published field observations associate this increase with frost flower growth and the capture of blowing snow by the flowers. To investigate the first part of this phenomenon, we carried out a laboratory experiment on the response of C band radar backscatter to frost flowers growing on the surface of newly formed saline ice. The experiment took place in a 5 m by 7 m by 1.2 m deep saline water pool located in a two-story indoor refrigerated facility at the Cold Regions Research and Engineering Laboratory. Sodium chloride ice was grown in this pool at an air temperature of −28°C. The frost flowers first appeared on the ice surface as dendrites and then changed to needles as the ice sheet grew thicker and the surface temperatures became colder. The frost flowers reached to a height of 10–15 mm, and beneath each cluster of frost flowers a slush layer formed to a thickness of approximately 4 mm. Far-field radar measurements of the backscatter from the ice were made at incident angles from 20° to 40° and at approximately 6-hour intervals throughout the 3-day period of the experiment. A backscatter minimum occurred early in the flower growth at the time coincident with an abrupt doubling in the ice surface salinity. Once the full flower coverage was achieved, we removed first the crystal flowers and then the slush layer from the ice surface. The results for these cases show that the crystals have little impact on the backscatter, while the underlying slush patches yield a backscatter increase of 3–5 dB over that of bare ice. The laboratory results suggest that this relative backscatter increase of approximately 5 dB can be used as an index to mark the full areal coverage of frost flowers.

1. Introduction

Frost flowers are fragile saline ice crystals which grow on the surface of young sea ice and are accompanied by the formation of a moist saline surface layer under the flowers. There are several motivations for the study of these flowers. First, the flowers appear frequently on thin ice during the Arctic cold season. *Perovich and Richter-Menge* [1994, p. 16,342], from field studies in the Beaufort Sea during March and April, observe that frost flower formation is "a normal step in the formation of sea ice under springtime conditions." Their observations show that it takes about 2 days from the initiation of ice growth for the flowers to cover the ice. *Martin* [1979] (S. Martin, private communication, 1996), during helicopter traverses over the Beaufort Sea in autumn and winter, observed a similar frequent occurrence of frost flowers on young ice.

Second, the flowers modify the thermal and surface properties of young sea ice. *Martin et al.* [1996] observe from laboratory experiments that the flowers insulate the solid ice surface from the cold atmosphere. They show that for air temperatures below −24°C, the infrared temperature of the flower tops is 4°–6°C colder than that of the solid ice. *Perovich and Richter-Menge* [1994] and *Ulander et al.* [1995] also show that additional surface modification occurs because the flowers and the saline surface capture blowing snow, which further alters the surface of the young sea ice.

Third, field observations suggest that the flower formation makes the ice appear brighter to microwave backscatter. For example, Figure 1 presents recent ERS 1 images showing a sequence of bright transient features occurring on the surface of young sea ice. Figure 1 shows that a transient increase of about 6 dB is associated with the young ice growth. Sea ice model analyses [*Nghiem et al.*, 1995] suggest that frost flowers are the cause of this enhanced radar backscatter. In other previous work, *Drinkwater and Crocker* [1988] study the dielectric and scattering properties of young snow-covered sea ice, and they also summarize historic observations of the flowers and the saline surface layer. From data taken during November–December in the Canadian Arctic they briefly describe the flower formation and the modification of the flowers by strong winds and snow deposition.

Perovich and Richter-Menge [1994] review more recent studies of the passive and active microwave signatures of young sea ice associated with these surface changes. They also give a detailed description of flower growth in the field and describe the dependence of the growth habit on air temperature. *Ulander et al.* [1995], from an August–September cruise to the north pole, compare backscatter values calculated from field observations of surface properties of several young sea ice sites

[1]Center for Space Microelectronics Technology, Jet Propulsion Laboratory, California Institute of Technology, Pasadena.
[2]School of Oceanography, University of Washington, Seattle.
[3]U.S. Army Cold Regions Research and Engineering Laboratory, Hanover, New Hampshire.

Copyright 1997 by the American Geophysical Union.

Paper number 96JC03208.
0148-0227/97/96JC-03208$09.00

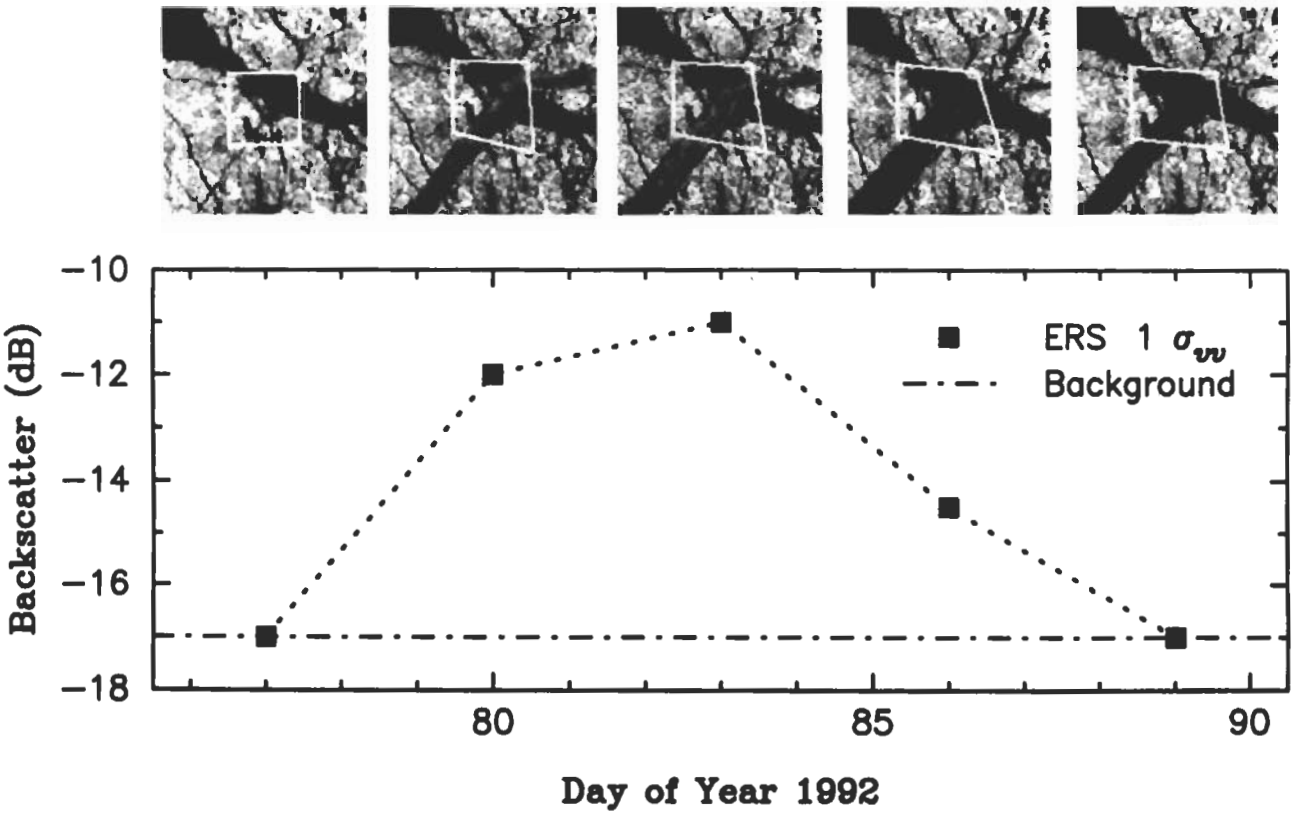

Figure 1. Series of ERS 1 images of a lead in the Beaufort Sea and a plot of ERS 1 backscatter for the area inside the lead where backscatter is enhanced by up to 6 dB above the background and then reduced again to the background backscatter level over a period of 12 days.

with ERS 1 synthetic aperture radar (SAR) observations for the same sites. They observe backscatter increases of 5–10 dB, with the largest increases occurring for snow-infiltrated flowers.

In the laboratory, *Martin et al.* [1995, 1996] show that frost flowers consist of ice crystals with characteristic heights of 10–30 mm, which grow on top of a patchy and highly saline 1- to 4-mm-thick slush layer. They find that flowers grow for the following reasons: within the ice, the thermomolecular pressure gradient transports brine to the surface [*Dash et al.*, 1995], where it evaporates into the cold unstable convective boundary layer. The combination of evaporation and sublimation leaves a dense brine layer at the surface and forms a region of supersaturated vapor immediately above the ice. As *Martin et al.* [1995, 1996] show, the height of this region of supersaturated vapor in part determines the height to which the crystals grow. The other determining factor of the flower height and growth habit is the range of temperatures in the convective boundary layer. Following *Hallett and Mason* [1958], for boundary layer temperatures between −12°C and −16°C the flowers form as dendritic crystals; for temperatures between −16°C and −25°C the flowers consist of ice needles. For the crystals to form, both the supersaturation and the necessary temperature range are required.

The significance of the flower growth and the associated changes in the surface salinity to radar observations is that understanding these processes is a step toward explaining the large variability in the radar signature of newly formed ice. An understanding of this variability will lead to better geophysical interpretations of radar remote-sensing data and to the interpretation of the thin ice signature in terms of its physical properties. The rapidly changing backscatter signature associated with the changes on the young ice surface may also yield a way to estimate the areal coverage of thin ice and the nature of the insulating layer on the thin ice surface. Finally, this understanding will allow us to separate the thin ice signature from the similarly bright return produced by Bragg scatter from wind-roughened open water.

Given this background, the purpose of this study is to determine from a laboratory experiment the relation between the backscatter signature of young sea ice and the frost flower growth. In the experiment we grew sea ice for 3 days and observed the changes in ice physical properties and the backscatter. However, we did not attempt to model the observed snow infiltration of the flowers. The radar used in the study is a C band polarimetric scatterometer, which measures all linear polarizations including vertical (VV) and horizontal (HH), so that the work is applicable to the C band SARs flown on the following satellites: ERS 1 and ERS 2 (VV) and RADARSAT (HH). The work will also be applicable to the planned ENVISAT satellite, which will carry a polarimetric C band SAR designed to monitor the polar ice caps and the sea ice extent [*Gardini et al.*, 1995]. This SAR will have the polarimetric diversity to measure VV and HH simultaneously or cross polarization with different transmitted and received polarizations in quasi-simultaneous operation with VV or HH [*Gardini et al.*, 1995]. Such varieties in SAR polarizations necessitate the polarimetric aspect of this frost flower signature study. In the following, section 2 describes the laboratory setup, section 3 gives the measurements of the frost flower growth, section 4

presents the backscatter results, and section 5 summarizes our conclusions.

2. Description of the Experiment

The experiment took place in a large indoor refrigerated facility at the Cold Regions Research and Engineering Laboratory (CRREL). Figure 2 shows the facility. The room measures about 6 m by 7 m on the floor, is about 8 m or two stories high, and has refrigeration units mounted adjacent to the ceiling. The room is divided into two floors by a metal grating, where sections of the grating can be removed to provide access to the lower level. We entered the cold room at the upper level and descended to the lower level by a ladder. The air temperature in the room could be controlled to within 2°C.

A freezing pool occupied most of the area of the lower level except for a walkway and measured about 5 by 7 m in plan view and 1.2 m in depth. The pool was filled to a 0.9-m depth with a sodium chloride solution of 31 practical salinity units (psu). Because the sodium and chloride ions are the dominant components of salts in seawater (about 78% by weight [*Neumann and Pierson*, 1966]), we assume that characteristics of saline ice in our laboratory conditions are equivalent to those in the field. In fact, comparisons of laboratory sodium chloride ice and field sea ice show that their growth rates, temperature profiles, salinity profiles, brine volumes, desalination effects, crystallographic structures, and intercellular spacings are similar for the thickness range of young thin ice under consideration [*Arcone et al.*, 1986; *Nghiem et al.*, 1997]. Two catwalks extended across the pool; one ran along the wall, and the other divided the pool into two areas. As Figure 2 shows, the area labeled "test section" was reserved for the radar measurements, while the area labeled "coring section" was used for taking ice cores and flower and slush samples. Because these sections were subjected to the same cooling and shared the common under-ice water, we assume that the flower and slush layer properties were the same in both sections. Above the test section we removed the grating and mounted the radar on one end and a nadir-looking video camera at the other end. The video camera was connected to a computer, which took digitized images of the ice every half hour. The field of view (FOV) at the ice surface was about 0.5 m × 0.5 m. The illumination for the video was provided by six low-intensity floodlights mounted on the catwalks. As Figure 2a shows, four of these provided a low-angle uniform illumination field within the video FOV. Because of the low angle the translucent flowers were brighter than the background flat ice.

Figure 3 shows a photograph of the antenna, the RF circuitry box, and the positioner of the C band polarimetric radar system setup in the cold room. The diagonal horn antenna was mounted on two aluminum arms extending out from the positioner base. A video camera mounted adjacent to the antenna pointed in the antenna look direction was used to obtain visual images of targeted areas, which were displayed on a monitor outside the cold room. The RF circuitry was installed inside a temperature-controlled (25°C) box attached to the square frame fixed to the antenna. A motor was connected to the horizontal mounting axis of the antenna by a chain to drive the antenna incident direction. The whole structure was bolted to a ball bearing disk on the positioner base and was rotated in azimuth by another motor inside the base. The base was fixed on the upper floor, and the antenna looked down through an opening to the ice sheet on the lower floor. The antenna was located about 3 m above the ice sheet to satisfy the far-field condition. With this setup the antenna could be pointed at any incident and azimuth directions. The radar will be described in further detail in the Appendix.

One critical factor in the experiment was the avoidance of unwanted radar reflections and multipath effects. To this end, we used microwave absorber sheets to line the walls of the room, cover the catwalks and lights, and shield the University of Washington camera system. We isolated the antenna from the rest of the room with an anechoic enclosure so that the antenna perceived the room as an anechoic chamber. Part of this enclosure was removed to take the photograph shown in Figure 3, where the anechoic wall is visible as the black background behind the antenna. This arrangement allowed for a maximum blockage of reflections and multipath noises with a minimal number of anechoic sheets.

To avoid a pressure buildup in the water under the ice, we suspended a heating tape through the ice beneath the catwalk adjacent to the wall. During the experiment the tape was heated and checked periodically to make sure that the hole through the ice sheet remained open. In the present experiment, unlike earlier experiments of *Martin et al.* [1995, 1996], which were done in a much smaller room with cooling units within 1.5 m of the ice surface, we found that the frost flowers grew without the addition of moisture to the boundary layer above the ice. This greatly simplified our study.

Our experimental procedure was as follows: after arranging the radar and video camera, we set the room temperature at −2°C while using a submersible pump to circulate the water in the pool. As soon as the water temperature fell to within 1° of the freezing point, we stopped the circulator and further lowered the room temperature to −28°C to initiate the ice growth. Once the saline ice sheet started to form, we measured the ice and flower properties at 6- to 12-hour intervals throughout the experiment. As a precaution we minimized the number of entrances into the cold room and used a plastic drape to cover the door between the cold room and the external warm room, where controlling devices and computers were located.

Once the ice began to grow, we made the following measurements. First, we measured the ice thickness by taking samples. For thin ice we took these samples with knives or a hand saw; for thicker ice we used a coring device. Upon removal of a sample or core we immediately measured its thickness with a ruler and then melted down the core to determine its bulk salinity. Second, we photographed the ice surface, taking both detailed photographs of frost flowers and overall photographs of the general growth. Third, we determined the salinities of the flowers, slush layer, and the adjacent bare ice. We measured the flower salinity by removing them from the slush layer surface with a cold clean knife blade. Then, we measured the slush layer salinity by taking a sample with either the knife or a small spatula. Finally, we determined the bare ice salinity at a site away from the flowers by again using the knife to scrape off a surface sample. We measured the sample salinities using a hand-held optical salinometer which required only a few drops of liquid. Two independent salinometers were used and cross checked; the measurement accuracy is about 1 psu.

We determined the approximate thickness of the humidity layer by placing a piece of ice-covered dental floss through the ice. When the boundary layer was supersaturated, ice crystals grew on the floss. To obtain a rough measure of the supersaturation thickness, we cleaned the ice from the floss at 6- to 12-hour intervals and then measured the height to which ice

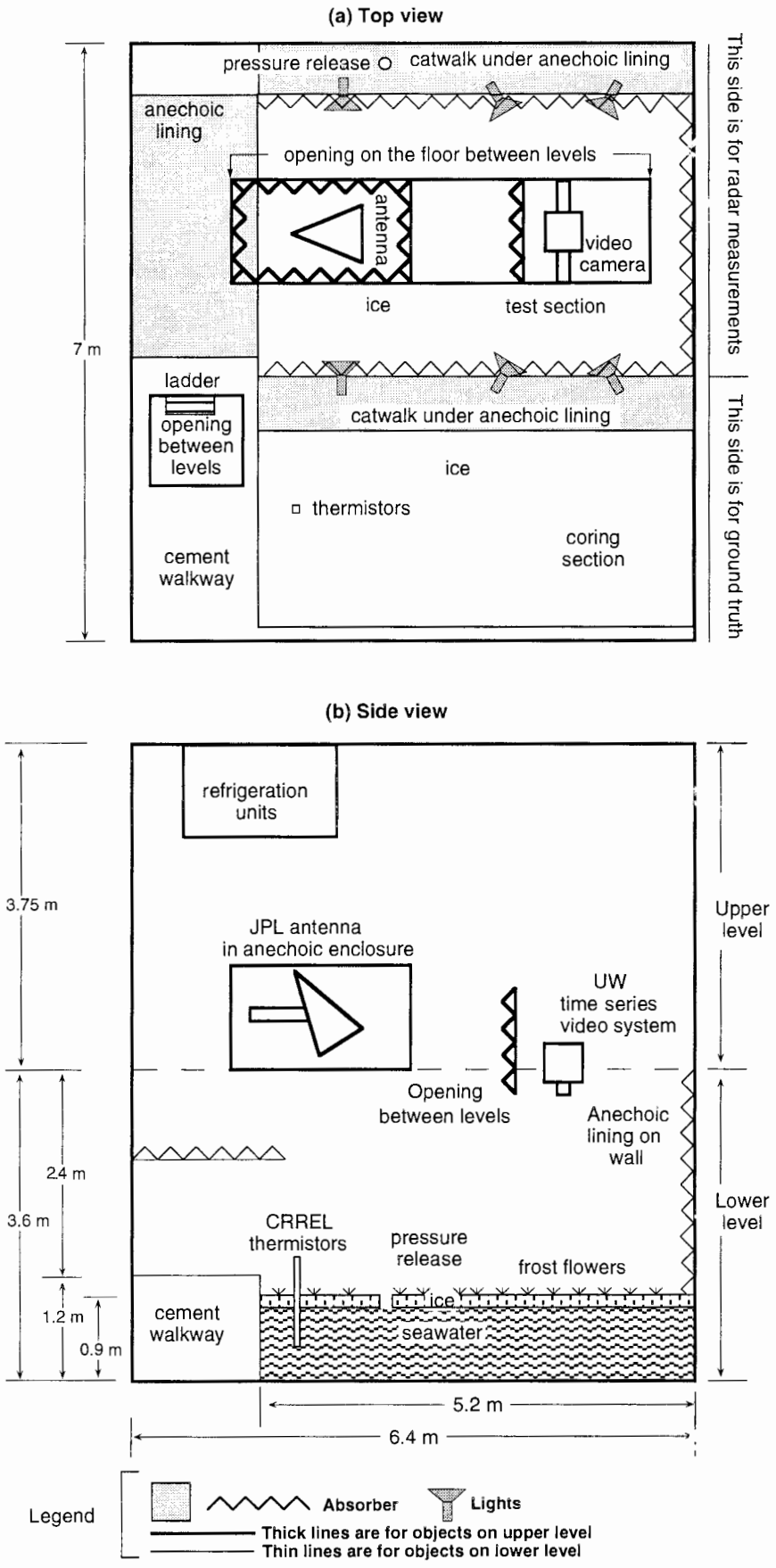

Figure 2. The laboratory setup in the CRREL cold room: (a) top view and (b) side view.

crystals regrow. In all cases this height was 30–40 mm. Finally, we determined the air and ice temperatures within the room in two different ways. First, air, ice, and water temperatures were recorded at 5-min intervals with a thermistor array mounted in a 2.5-cm-diameter polyvinyl chloride pipe. The thermistors were spaced at vertical intervals of 1 cm in the ice and 1 or 5 cm in the water. Air temperatures were measured at heights of 1, 2, 3, 4, and 9 cm above the ice surface. Because of the thermal conduction through the pipe, the accuracy of this temperature data series is below the desired value in regions of high-temperature gradients. Because of this we also used hand-held thermistors accurate to about 0.1°C to measure various ice and air temperatures. In addition, the air temperature was recorded as part of the refrigeration monitoring system.

The experiment lasted about 3 days, during which time the ice thickness grew to a 0.15-m thickness, or about 17% of the total depth, and the water salinity increased from about 31 to 35 psu. We terminated the experiment at 3 days to avoid further buildup of the salinity of the water under the ice and because at this time the flower areal extent reached what appeared to be its final coverage.

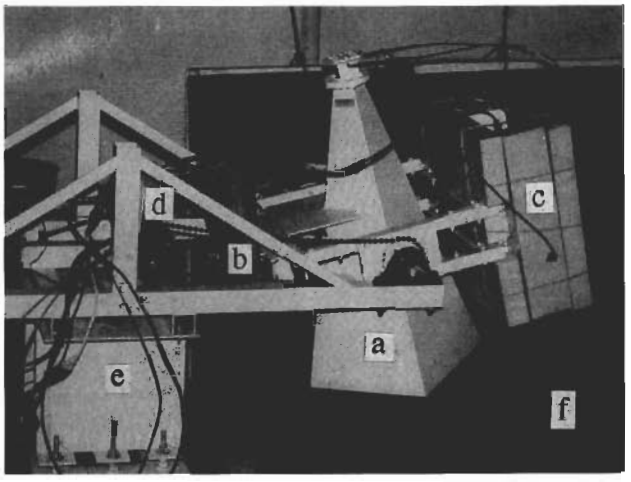

Figure 3. Photograph of the front end of the C band polarimetric scatterometer. The inset letters indicate a, diagonal horn antenna; b, video camera; c, RF box; d, motor for incident angle; e, base of the positioner; and f, wall of the anechoic enclosure.

3. Frost Flower Results

Plate 1 presents photographs and schematic drawings of the dendritic and needle flowers which formed in our experiment. *Perovich and Richter-Menge* [1994] observed both these flower types in their field studies. Plate 1a, a photograph of frost flowers taken with a hand-held camera at 9 hours from the start of the ice growth, shows that the first type of flowers to form on the ice surface was dendrites. The photograph also shows that the flowers are tilted to the left, which is opposite to the direction of a weak surface air current. The slush layer is apparent at the left side of the photograph. The inset figure indicates that the flowers were about 10–20 mm high, at the time when the height of the supersaturated region was about 40 mm, and the slush layer thickness was about 2–4 mm. Except at the very beginning of the experiment when small isolated flowers started to formed, the slush layer always occurred under the frost flowers. On the bare ice surface outside the flower clusters the slush layer did not exist. The inset shows the temperatures taken with the hand-held thermistor. We note that in this experiment, temperature measurements at the flower tops were difficult and subject to a larger uncertainty compared to measurements of surface temperatures. We found that the air temperature at the top of the flowers was about −21°C, and the temperature below the flowers within the slush layer was about −11°C. Although the flower top temperature is too cold, the slush layer temperature is consistent with dendritic flower growth.

Later in the experiment, between about 48 and 55 hours, we observed that the dendrites slowly evolved into needles. Plate 1b, a photograph of these needles at 52 hours, shows that the needles had a length of about 10 mm and a diameter less than 1 mm. Similar changes occur in studies of pure crystal growth, where moving a crystal from one temperature regime to another leads to a change in its growth habit [*Hallett and Mason*, 1958]. In our constant room temperature experiment, the reason for this change is that the surface temperature decreases as the ice thickness increases. This decrease in ice surface temperature with increasing thickness means that the initial conditions favor dendritic crystals and that needles form later. The inset shows that the needles had a temperature at the top of the slush layer of −17°C and a flower top temperature of −25°C. These observations suggest that the transition from dendrites to needles is associated with cooling of the ice surface caused by the ice thickness increase.

Another observation from the insets in Plate 1 is that the ice surface temperatures under the slush layer were about 8°–10°C warmer than the temperatures of the adjacent bare ice. *Martin et al.* [1996] show from infrared radiometer measurements that the cause of this temperature difference is the insulating effect of frost flowers.

To show the overall flower growth in the radar test section, Plate 2 presents a sequence of oblique photographs of the ice surface taken from the cement walkway beneath the radar. The times of these photographs immediately preceded the times of polarimetric radar data acquisitions. The bright flares in the pictures were reflections from the lights. A 10-cm scale placed on the ice within the video FOV is also visible in the upper right-hand portion of Plates 2a and 2b. In the subsequent panels the intersection of the cross of lights near the top of the photographs also shows the location of the video FOV.

Figure 4 shows video images of the flower growth at 4-hour intervals throughout the experiment, beginning at an elapsed time of 16 hours. The 10-cm ruler in the lower left provides a scale and the clock gives the local time. Since the experiment began at 12 noon local time, the elapsed times in the first three images equal the clock time plus 12 hours. Figure 4 shows that as in previous work by *Martin et al.* [1995, 1996], the flowers covered the ice by colonization of new sites and by lateral growth from existing sites. The flowers began as individual small crystals with no slush underneath. As the crystals grew laterally into clusters, the slush layer formed and increased in thickness beneath the flowers. An examination of the sequential images shows that the flower clusters grow from lower left to upper right. When we used small paper wind vanes to examine the air flow over the region, we found that the sample region was characterized by a weak steady surface air current flowing against the growth direction. This suggests that the air current carries the humidity supersaturation toward the flowers, which remove the supersaturation by their upwind growth. Regarding the overall growth, a comparison of Plate 2 and

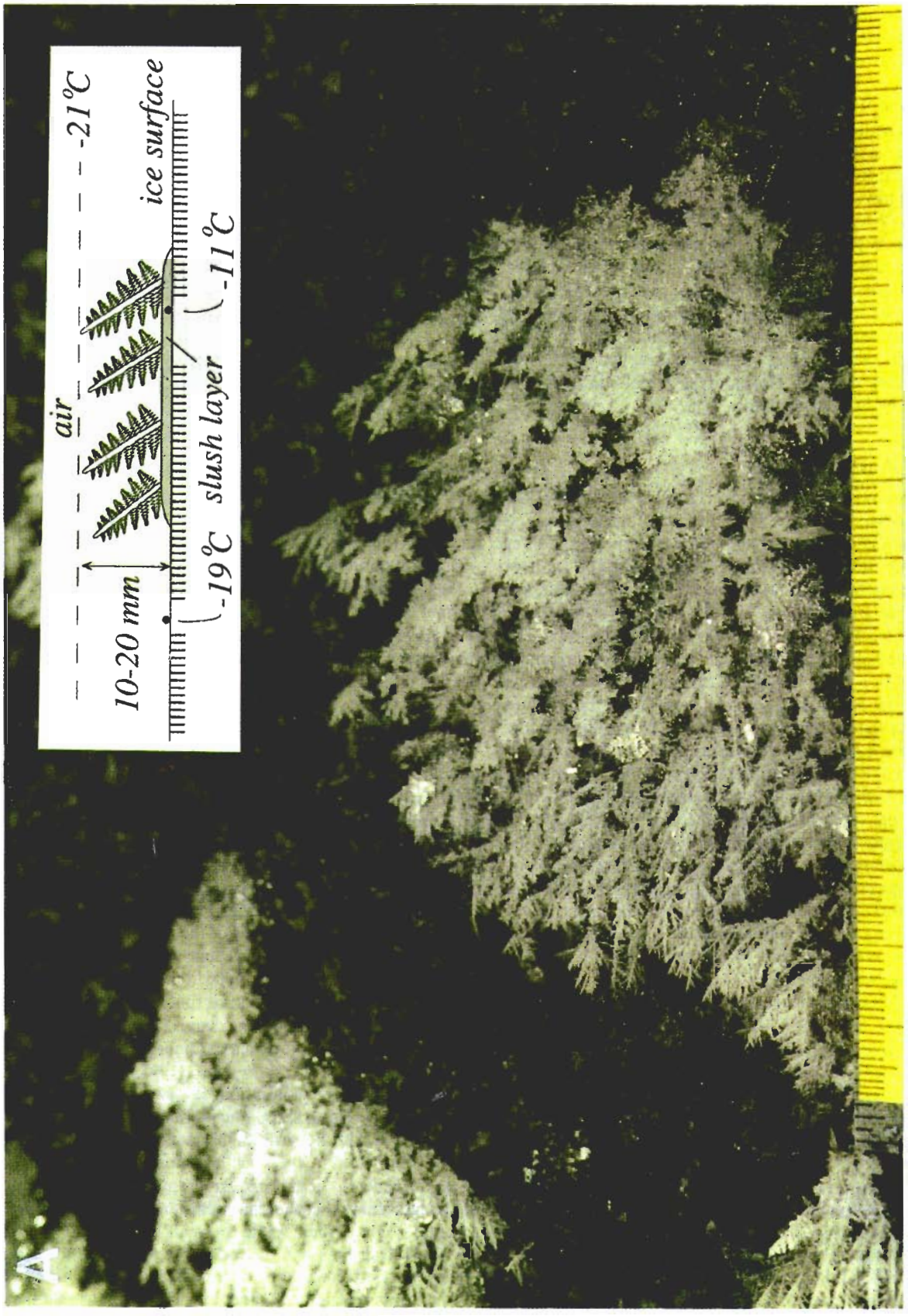

Plate 1. Photographs of the two kinds of frost flower observed in the experiment: (a) stellar dendrite crystals taken at 9 hours and (b) needle crystals taken at 52 hours. The insets in each plate show a schematic view of the flowers, slush layer, and temperatures measured at different parts of the flowers.

Plate 1. (continued)

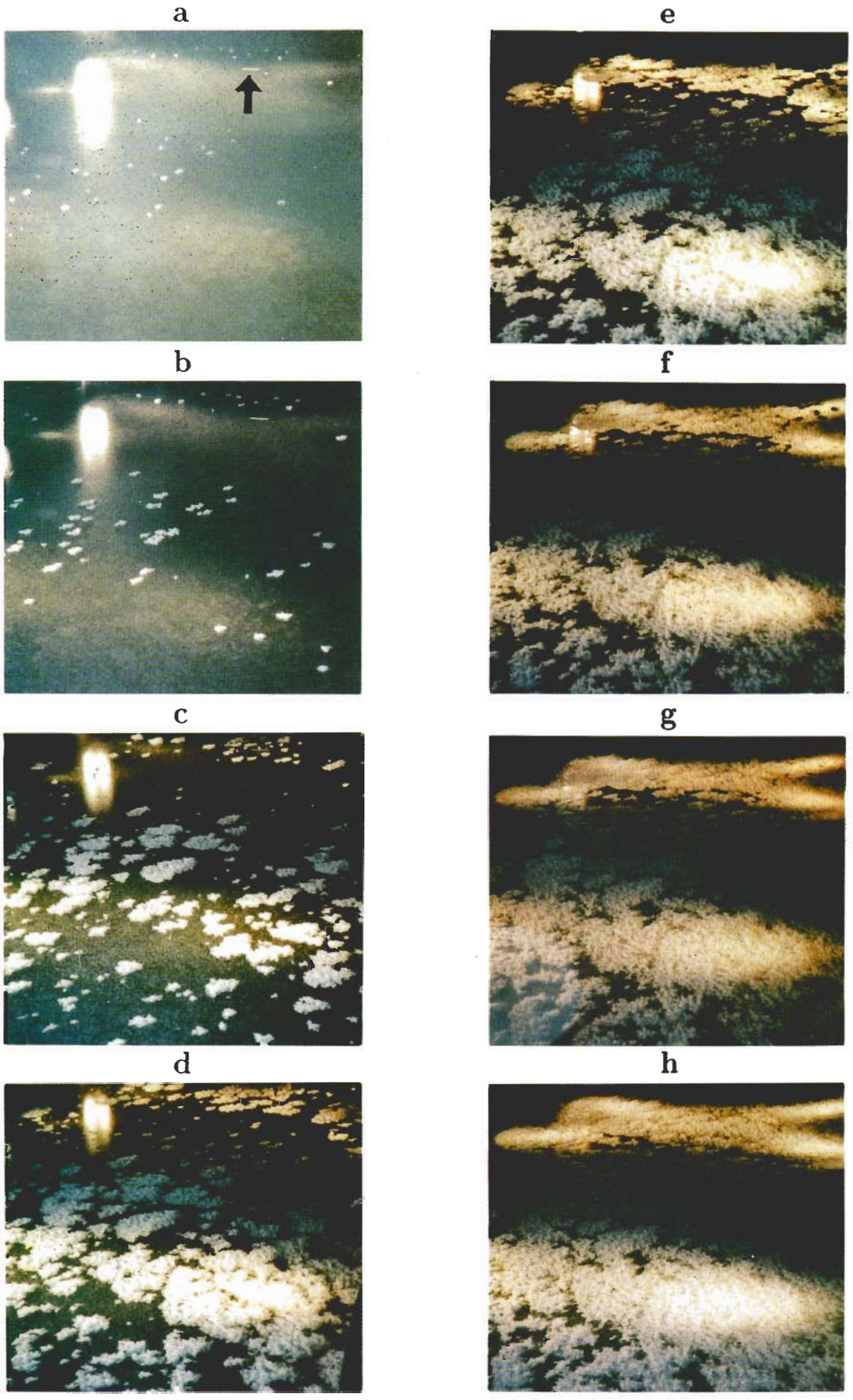

Plate 2. A sequence of photographs taken beneath the radar looking toward the video FOV, at times close to the polarimetric radar data acquisitions. The FOV is near the right side of the upper part of the photographs where the ruler is seen as a short white horizontal object, indicated by the arrow in Plate 2a. Elapsed times are (a) 6 hours, (b) 12.25 hours, (c) 25 hours, (d) 34 hours, (e) 43 hours, (f), 50.25 hours, (g) 56 hours, and (h) 68.5 hours.

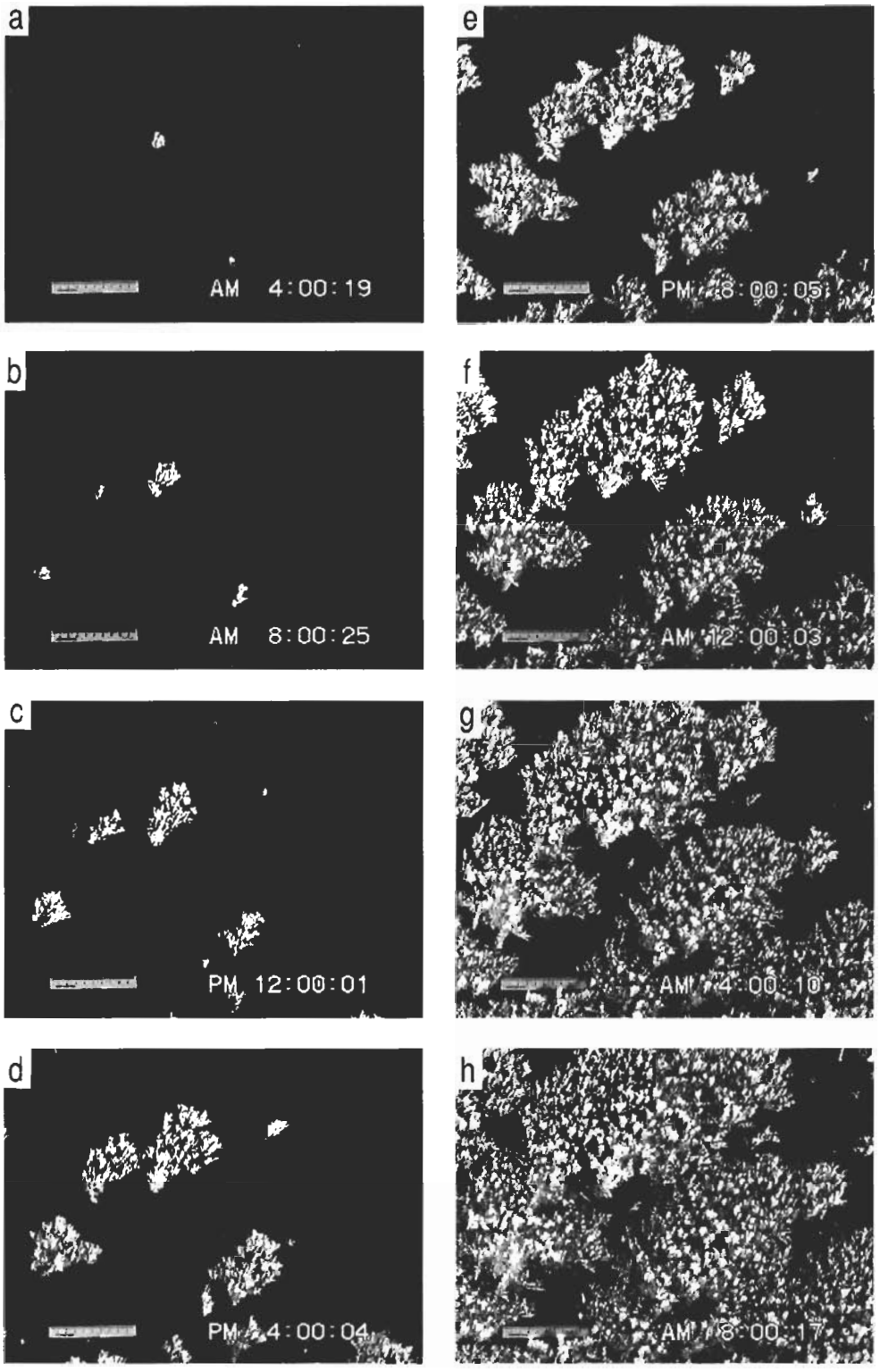

Figure 4. Sequence of video images showing the growth of frost flowers at 4-hour intervals starting at 0400 local time, which corresponds to an elapsed time of 16 hours. The 10-cm ruler shown at the lower left provides a scale for the images.

Figure 4 shows that the flowers in the video FOV formed about 6 hours after the initial flower formation in the area closer to the radar. Finally, both Plate 2 and Figure 4 clearly show the patchy nature of the frost flower coverage.

For each video image we used a simple intensity threshold filter to derive the relative area of bare and flower-covered ice. Figure 5a presents the increase in areal coverage with time. Figure 5a shows that the flower growth began slowly, increased, and then slowed as it reached its equilibrium value. On Figure 5a, vertical arrows "a" and "b," mark two different times. Arrow a indicates the time at which the surface salinity increased abruptly (discussed below in Figure 6), and arrow b

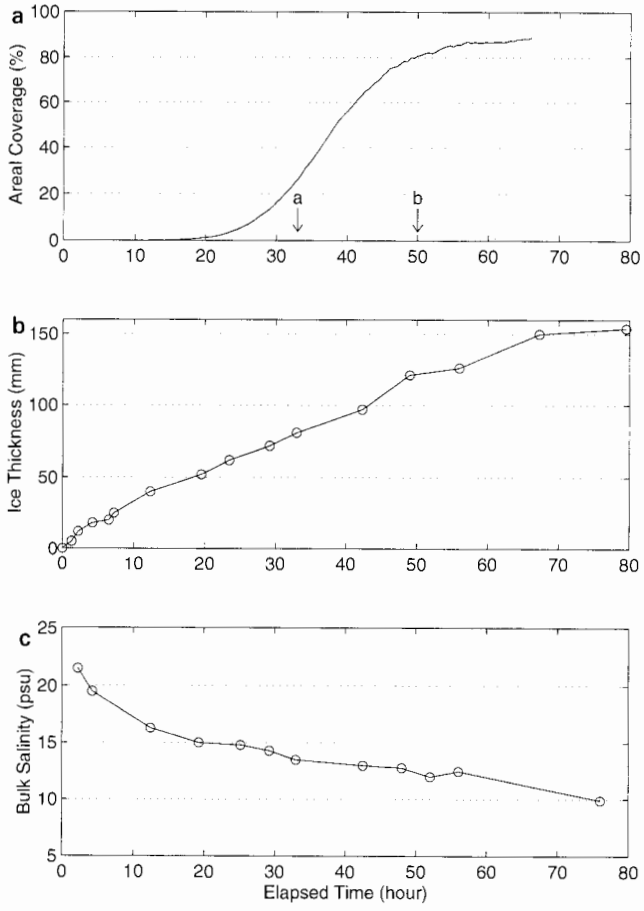

Figure 5. Changes with time of the ice and flower characteristics: (a) the areal flower coverage, (b) the ice thickness, and (c) the bulk salinity.

is the approximate time of the transition from dendrites to needles. Figure 5a shows that neither of these events appear to affect the areal growth. For other ice properties, Figure 5b shows the increase in ice thickness, and Figure 5c plots the decrease in the bulk salinity of the ice. Figures 5a–5c show that as the areal extent of the flowers increased from 0 to 90%, the ice thickness increased from 50 to 150 mm, and the bulk salinity slowly decreased from 15 to 11 psu.

Throughout the experiment, as described in section 2, we also measured the salinities of the slush layer, frost flowers, and bare ice surface surrounding the flowers. Figure 6, a plot of the time series of these observations, shows that the surface salinity began with values of 16–34 psu, until an elapsed time of about 32 hours. At this time the surface salinity effectively doubled to a value of 50–80 psu. For the same period the flower salinity began at 47 psu and then increased with time to a maximum value of 120 psu. The slush layer salinity also initially increased with time but remained smaller than the frost flower salinity and larger than the bare surface salinity. In general, the slush and flower salinities were about 50 psu larger than the bare surface salinity.

Between 68 and 71 hours we made two measurements of the liquid equivalent of the flowers and slush layer. We did these measurements by measuring out rectangles on the ice with dimensions of 150 × 150 mm^2 and 130 × 140 mm^2, collecting all the surface material within each rectangle, and melting it down. The first measurement gave 1.0 mm liquid equivalent per unit area; the second gave 1.7 mm. These numbers are consistent with *Martin et al.* [1996], who observed thicknesses of 1–2 mm. In summary, the effect of the frost flower clusters is to create a patchy surface coverage of slush with layer thicknesses of 2–4 mm, where the patch salinity is about 50 psu larger than that of the bare ice.

The patchy surface coverage which we observe is not unique to our laboratory experiment. It also occurs at what appear to be similar scales in the field photographs of frost flowers by *Perovich and Richter-Menge* [1994, Figure 2] and in the photographs of flowers and snow-infiltrated flowers by *Ulander et al.* [1995, Figures 6 and 7a]. This suggests that our results are applicable to field studies.

4. Radar Observations of Frost Flowers

4.1. Observations During the Frost Flower Growth

We present data at the C band frequency of 5 GHz for incident angles at 20° to 40°. Note that this range of incident angle overlaps both the ERS incident angle range (19°–26°) and the RADARSAT range (20°–49°). As Plate 2 shows, the frost flower cover at different radar ranges on the ice sheet was not uniform. Consequently, to determine the trend of microwave interactions with the frost flowers during ice growth, measured values of backscatter at different times should be compared at fixed incident angles. The nonuniformity also introduces more variability in the data since a limited number of azimuth samples are obtainable due to the temporal and

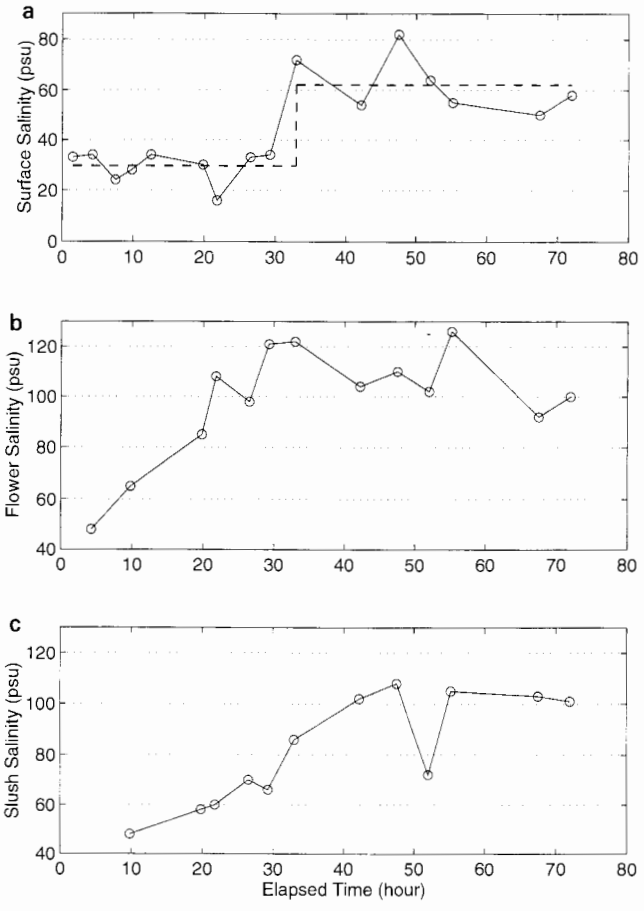

Figure 6. The time dependence of the salinities of (a) the bare ice surface, (b) the frost flowers, and (c) the slush patches.

spatial limitations of the experimental facility. Figure 7 presents backscatter observations versus elapsed time for horizontal (σ_{HH} denoted by squares), vertical (σ_{VV} denoted by triangles), and cross polarizations (σ_{HV} denoted by crosses) for incident angles at 25°, 30°, 35°, and 40°.

The first backscatter data set in Figure 7 was taken when the ice sheet was 2 cm thick and flowers had just started to appear. At this time, only a small number of isolated frost flowers formed on the ice surface as seen in Plate 2a, and the backscatter was low for all polarizations. As the ice became thicker with an increasing flower coverage (see Plate 2 and Figure 4), both the horizontal and vertical backscatter signatures in Figure 7 show an increase in magnitude, followed by a definite minimum at about 35 hours.

An exception is at 40° where the minimum seems to occur at a later time; note that the frost flower area corresponding to this incident angle was at the far end of the ice sheet where the flowers formed more slowly than those closer to the radar. The cross-polarized return also exhibits this minimum at 30° and 35° incident angles. However, the uncertainty in σ_{HV} is larger compared to those in the copolarized returns due to a lower signal-to-noise ratio of the cross-polarized measurements, and the minimum in the cross-polarized returns is not conclusive (for example, see error bars in Figure 7b for σ_{HV} at 30°).

An examination of Figure 6a shows that the time of the backscatter minimum coincides with the time at which the surface salinity doubles. We note that while the minimum occurred in the radar backscatter, aside from the salinity doubling, no other change was visible in the nadir-looking optical video images nor in the video tape recorded by the antenna-mounted camera. Other measurements of the flower and slush salinities, and the crystal structure, also show no significant change at this time.

4.2. Effects of Frost Flower Constituents on Polarimetric Backscatter

Near the end of the experiment the frost flower coverage reached more than 90%, as observed in Plate 2 and Figure 4, over a 15-cm-thick ice sheet. To determine the relative backscatter contributions from the crystal flowers and the slush layer, we carried out three sets of polarimetric scatterometer measurements.

The first set was done with the flower and slush layer coverage left intact. Then, we removed only the crystal flowers. We carried out this tedious operation by disassembling the lights and radar absorbers, lying down on the catwalk, and then rolling it incrementally across the ice surface while we removed the flowers with a knife blade. This procedure left only the slush patches on the ice surface. We then reassembled the lights and absorbers and, beginning about 1 hour after clearing the flowers, took a second set of backscatter data from the slush layer. About 4 hours after completion of this measurement, we used large sharp paint scrapers and plastering tools to skim away the slush layer from the ice. One to two hours later, we collected a third set of radar data from the bare ice. Because the earlier infrared radiometer measurements of *Martin et al.* [1996] show that clearing the flowers causes the greatest change in the surface temperature, while clearing the slush layer has only a negligible effect, this procedure should have allowed sufficient time for the bare ice surface temperature to equilibrate with the air.

At the final stage of frost flower growth, the study as a function of incident angle is more appropriate because of an approximately full coverage of frost flowers at this stage of the experiment alleviating the inhomogeneities at the different incident angles. Figure 8 presents results of the mean backscatter for the above three cases at incident angles from 20° to 40°. First, for the case of full frost flowers, σ_{HH} decreases by 6 dB over the range of incident angles, while the change in σ_{VV} versus incident angles is only within 2 dB.

Next, we compare the backscatter from the full flower case with the case of flower crystals removed. For the vertical polarization the backscatter with flower crystals removed is slightly higher (around 1 dB) than the case of full frost flowers (top panel of Figure 8, except at 40°), which may indicate an attenuating effect of the crystals. The differences are, however, within the relative uncertainties (approximately ±1 dB) of the two cases. Similarly, the changes are within measurement uncertainties for both the horizontal backscatter (middle panel of Figure 8) and the cross-polarized return (bottom panel of

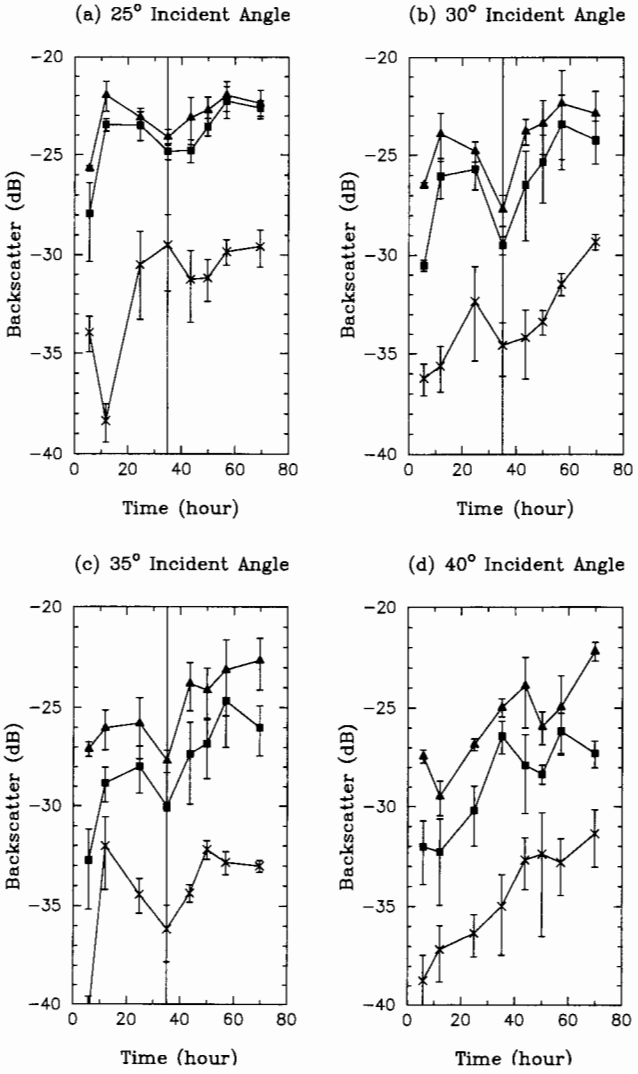

Figure 7. Changes in backscatter during the process of frost flower formation on the thin ice sheet for incident angles from 25° to 40°. Triangles are backscatter data for σ_{VV}, squares are for σ_{HH}, and crosses are for σ_{HV}. The dips in backscatter at different incident angles are marked with the vertical lines, which coincide with the time when salinity of the bare ice surface jumped by a factor of 2.

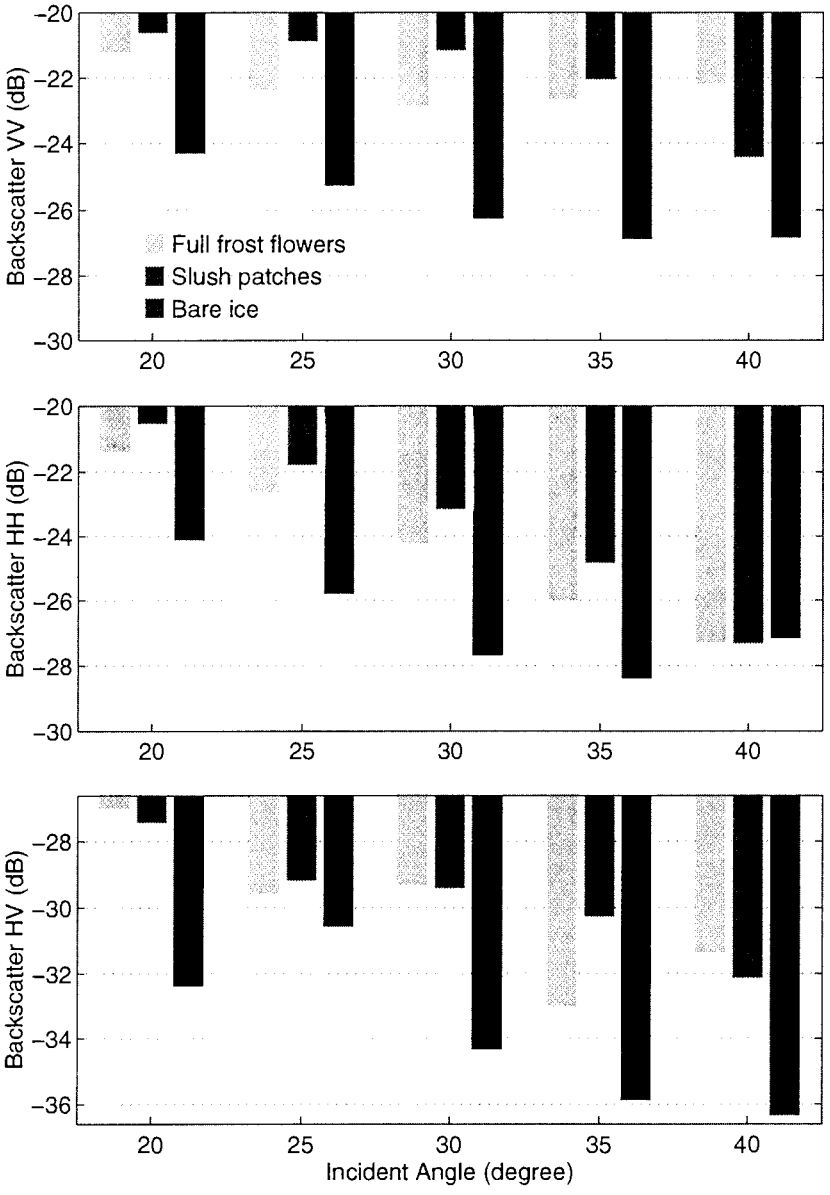

Figure 8. Comparisons of backscatter σ_{VV}, σ_{HH}, and σ_{HV} for the full frost flower formation (about 90% in areal coverage), for slush patches exposed by removing flower ice crystals in the frost flower formation, and for the bare ice with all slush patches also removed.

Figure 8). We conclude that the fragile flower crystals have little impact on the microwave backscatter.

Compared to the bare ice case, Figure 8 shows that the full flower backscatter is 3–5 dB higher for all polarizations. These comparisons show that the patchy slush layer contributes significantly to the backscatter. The observed difference in backscatter between the full flower and the bare ice cases gives a quantitative estimate of the backscatter enhancement caused by the frost flower formation. Furthermore, a comparison of the bare ice backscatter with similar measurements, made 2 years earlier at CRREL by *Nghiem et al.* [1995], shows that the backscatter from the bare ice sheets is comparable. This confirms the experimental repeatability.

To further examine the backscatter signatures, we present full polarimetric measurements including copolarized ratio in Figure 9a, cross-polarized ratio in Figure 9b, magnitude of ρ in Figure 9c, and phase of ρ in Figure 9d for the three cases. Copolarized ratios $\gamma = \sigma_{VV}/\sigma_{HH}$ of these cases are similar at incident angles from 20° to 30° as shown in Figure 9a. At larger incident angles (35°–40°) the full frost flower case has the largest copolarized ratio and the bare ice has the smallest. For the case where the flower crystals are removed, the copolarized ratio seems to decrease slightly compared to the full frost flower case. For cross-polarized ratios, there is no systematic trend in the data. Magnitudes of the complex correlation coefficient ρ are between 0.8 and 0.9, phases of ρ are about 0°, and there is no definitive differences in ρ for these cases.

Finally, we compare our laboratory backscatter measurements with those made in the Beaufort Sea by the ERS 1 C band SAR. The SAR data are extracted from the large and long lead seen in Figure 1. The boxes in the SAR images are determined by the same four points for the corners, and it is used to show the opening and closing of the lead. In general, the backscatter of frost flower–covered ice in the laboratory

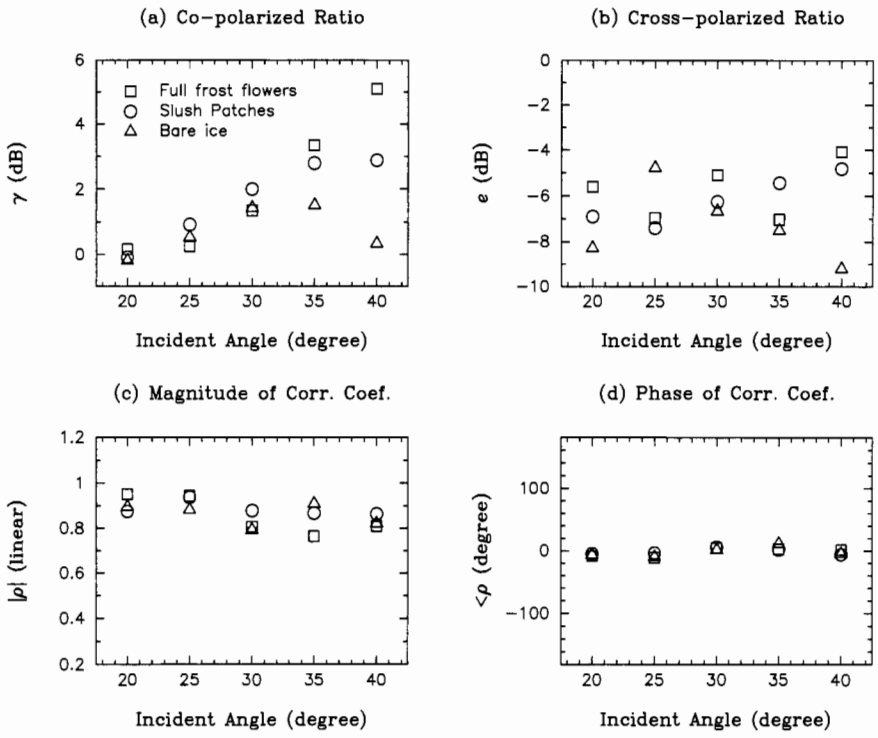

Figure 9. Comparisons of (a) copolarized ratio, (b) cross-polarized ratio, (c) magnitude, and (d) phase of the polarimetric complex correlation coefficient between horizontal and vertical returns. These are for the full frost flower formation (about 90% in areal coverage), for slush patches exposed by removing flower ice crystals in the frost flower formation, and for the bare ice with all slush patches also removed.

increases by 3–5 dB (Figure 8), and the increase in the ERS 1 backscatter is 2.5–6 dB above the background (Figure 1). This is also comparable to an approximately 5-dB increase in copolarized backscatter predicted by *Nghiem et al.* [1995] for a 100% flower coverage. At 20° incident angle, frost flowers on the laboratory grown ice give about 3 dB increase in σ_{VV}, which is within the range of backscatter enhancement at the early stages of frost flower growth in the ERS 1 images. Note that while the laboratory and field backscatter increases above the background backscatter levels are comparable, the values of the backscatter from the background ice sheets in the two cases are different due to differences in thickness, temperature, brine volumes, or surface roughness of the underlying ice sheets.

We have presented results of backscatter signature corresponding to the early growth phase of frost flowers on thin sea ice; however, we have not addressed the decay phase of the frost flowers as seen in the late stages in Figure 1. Also, as *Ulander et al.* [1995] suggest, a cause of larger changes that occur with time in ERS 1 backscatter may be due to blowing snow captured by the flowers, which may cause an enhanced surface roughness and a greater backscatter increase.

5. Conclusions

The paper presents results of a laboratory investigation of the effect of frost flower growth on C band radar backscatter. During the experiment the flowers first grew as dendrites and then transformed to needles. This transformation is associated with a cooling of the temperatures in the atmospheric boundary layer. As the experiment progressed, a patchy slush layer with high salinity formed beneath the flowers. The experiment achieved a final areal flower coverage of as much as 90%.

Early in the experiment when the areal coverage of frost flowers was below 30%, the ice surface salinity abruptly doubled and a minimum occurred in backscatter at incident angles from 25° to 35°. No significant change in the backscatter occurred either during the transition from dendrites to needles or when at the end of the experiment we removed the flower ice crystals, leaving only the slush patches. Both observations are consistent with the fact that the ice crystals have little effect on the backscatter, so that the slush patches are the major contributor to the observed backscatter changes.

Polarimetric backscatter data indicate that the flower-covered ice has a higher copolarized backscatter ratio γ compared to the case of bare ice in the range of incident angles from 35° to 40°. No systematic trend is observed in the cross-polarized backscatter ratio e, and the flowers had little effect on the complex correlation coefficient ρ between the copolarized returns. At the end of the experiment, comparisons of backscatter for the case of ice covered by the frost flower formation to the case of bare ice with all frost flowers and slush patches removed show that the flower and slush coverage causes an increase of 3–5 dB in backscatter above the background ice radar returns. This backscatter increase is consistent with ERS 1 observations of the backscatter enhancement in a Beaufort Sea lead. As a check, backscatter from this bare ice sheet consistently compares with that of another bare ice sheet measured 2 years earlier.

For geophysical applications of radar remote sensing this experiment suggests that the strong backscatter increase of the order of 5 dB, over the background radar return from thin ice, can be used as an index to mark the nearly full coverage (90% areal fraction) of frost flowers. This backscatter increase also

serves as an indicator of the environmental conditions that promote the growth of frost flowers. In this respect, Figure 1 illustrates the utilization of time series spaceborne radar backscatter for such geophysical applications.

The paper, however, leaves several questions unanswered. First, there is no published field investigation which describes the existence and nature of the slush layer associated with frost flowers, although anecdotal evidence exists. Second, the specific problem of the impact of blowing snow on the flowers, on the heat transfer, and on the radar backscatter is important and remains to be studied. Third, in the field, thin ice is also subject to rafting, ridging, and deformation, where these effects need to be incorporated into the backscatter model. Our present study is valid for the early growth of the frost flowers and shows the important role of the slush layer in the backscatter enhancement. Beyond this early growth stage, further laboratory and field experiments are necessary to determine the development and decay of the transient thin sea ice signature.

Appendix: Scatterometer Setup and Operations

We describe here the scatterometer setup and operations pertaining to this experiment and refer the scatterometer system and antenna characteristics to *Nghiem et al.*'s [1997] paper. The C band system operated at a center frequency of 5 GHz with a 1-GHz bandwidth and a 12° beam width. During calibration, one wall of the anechoic enclosure around the antenna was removed, and the antenna was pointed away from the ice toward a bright calibration target set up in the radar far field on one side of the upper floor. The target was positioned on a Styrofoam pedestal against an absorber background. For each set of calibration measurements, two types of calibration targets were used: a trihedral corner reflector and a metallic sphere.

In the setting of the antenna pointing direction the operator adjusted the remote azimuth and incident angle (0.05° accuracy) controllers until the desired direction was obtained. Using the video camera mounted with the antenna, the operator viewed the targeted areas on a monitor. These video observations of the ice conditions along with verbal comments by the operator were recorded to VCR tapes in addition to our written comments in the log. In the warm room the operator used a computer to control the scatterometer and the data acquisition system.

During the experiment we took polarimetric scattering matrix measurements at approximately 6-hour intervals. No one was permitted to enter the room during these measurements. Radar data were taken for incident angles from 0 to 45°, each with four independent azimuthal angles. For each incident and azimuth angle, 20 sets of measurements with 401 frequency samples were collected and coherently averaged. Processed data consist of polarimetric backscattering coefficients including σ_{HH}, σ_{VV}, and σ_{HV} and magnitude and phase of σ_{HHVV}. Measured off-diagonal elements in the 2×2 scattering matrix were within 0.15 dB in magnitude and 3° in phase of each other, which practically satisfies the reciprocity principle. Ideally, the reciprocity requires a balance of 0.0 dB in magnitude and 0° in phase for these scattering elements.

To check for coherent contamination from the antenna sidelobe return from nadir, we made measurements both with and without absorber sheets covering the surface beneath the antenna with an area equivalent to the antenna nadir footprint. If the backscatter measured at an oblique incident angle remained unchanged with and without the absorbers, then the incoherent backscatter measurement at this angle was not affected by the normal coherent reflection from the ice surface. From measured data we determined that data at incident angles less than 15° contained the coherent effect. Thus in section 4 we present data for incident angles at 20° or larger (to 40°), which are free from the coherent error source.

Acknowledgments. The research described in this paper was performed by the Center for Space Microelectronics Technology, Jet Propulsion Laboratory, California Institute of Technology, and was sponsored by the Office of Naval Research (ONR), through an agreement with the National Aeronautics and Space Administration. The research by the University of Washington was under ONR contract N00014-90-J-0161, and the research by the U. S. Army CRREL was under ONR contracts N00014-95-MP-3002 and N00014-95-MP-3019. John Govoni's and Bruce Elder's help in setting up the CRREL facility is very much appreciated. The assistance of K. H. Ding of the Massachusetts Institute of Technology in the scatterometer data acquisition is acknowledged. We thank J. A. Richter-Menge of CRREL for her constructive comments in the review of the paper.

References

Arcone, S. A., A. J. Gow, and S. McGrew, Microwave dielectric, structural, and salinity properties of simulated sea ice, *IEEE Trans. Geosci. Remote Sens.*, *GE-24*(6), 832–839, 1986.

Dash, J. G., H. Fu, and J. S. Wettlaufer, The premelting of ice and its environmental consequences, *Rep. Prog. Phys.*, *58*, 115–167, 1995.

Drinkwater, M. R., and G. B. Crocker, Modelling changes in the dielectric and scattering properties of young snow-covered sea ice at GHz frequencies, *J. Glaciol.*, *34*, 274–282, 1988.

Gardini, B., G. Graf, and G. Ratier, The instruments on ENVISAT, *Acta Astronaut.*, *37*, 301–311, 1995.

Hallett, J., and B. J. Mason, The influence of temperature and supersaturation on the habit of crystals grown from the vapor, *Proc. R. Soc. London A*, *247*, 440–453, 1958.

Martin, S., A field study of brine drainage and oil entrainment in first-year sea ice, *J. Glaciol.*, *22*, 473–502, 1979.

Martin, S., R. Drucker, and M. Fort, A laboratory study of frost flower growth on the surface of young sea ice, *J. Geophys. Res.*, *100*(C4), 7027–7036, 1995.

Martin, S., Y. Yu, and R. Drucker, The temperature dependence of frost flower growth on laboratory sea ice and the effect of the flowers on infrared observations of the surface, *J. Geophys. Res.*, *101*(C5), 12,111–12,125, 1996.

Neumann, G., and W. J. Pierson Jr., *Principles of Physical Oceanography*, Prentice-Hall, Englewood Cliffs, N. J., 1966.

Nghiem, S. V., R. Kwok, S. H. Yueh, J. A. Kong, C. C. Hsu, M. A. Tassoudji, and R. T. Shin, Polarimetric scattering from layered media with multiple species of scatterers, *Radio Sci.*, *30*(4), 835–852, 1995.

Nghiem, S. V., R. Kwok, S. H. Yueh, A. J. Gow, D. K. Perovich, J. A. Kong, and C. C. Hsu, Evolution in polarimetric signatures of thin saline ice under constant growth, *Radio Sci.*, in press, 1997.

Perovich, D. K., and J. A. Richter-Menge, Surface characteristics of lead ice, *J. Geophys. Res.*, *99*(C8), 16,341–16,350, 1994.

Ulander, L. M. H., A. Carlstrom, and J. Askne, Effect of frost flowers, rough saline snow and slush on the ERS-1 backscatter of thin Arctic sea-ice, *Int. J. Remote Sens.*, *16*(17), 3287–3305, 1995.

R. Drucker and S. Martin, School of Oceanography, University of Washington, Box 357940, Seattle, WA 98195-7940.

A. J. Gow and D. K. Perovich, U.S. Army Cold Regions Research and Engineering Laboratory, Hanover, NH 03755.

R. Kwok and S. V. Nghiem, Center for Space Microelectrics Technology, Jet Propulsion Laboratory, California Institute of Technology, Mail Stop 300-235, Pasadena, CA 91109. (e-mail: nghiem@malibu.jpl.nasa.gov)

(Received June 4, 1996; revised October 3, 1996; accepted October 7, 1996.)